Journal of Fluids and Structures 67 (2016) 22–33

Contents lists available at ScienceDirect

Journal of Fluids and Structures

journal homepage: www.elsevier.com/locate/jfs

Experimental assessment of performance characteristics for pitching flexible propulsors

Brendan C. Egan, Cody J. Brownell *, Mark M. Murray

United States Naval Academy, 590 Holloway Road, Annapolis, MD 201402, United States

ARTICLE INFO

Article history:
Received 6 May 2015
Received in revised form
2 September 2016
Accepted 9 September 2016

Keywords:
Biological fluid dynamics
Hydroelasticity
Propulsion
Swimming
Flexible propulsor

ABSTRACT

Using a flexible hydrodynamic foil that pitches to produce thrust, the most pertinent aspects of a fish-like propulsion system are replicated in a controlled environment. The pitching and flexing combination creates a hydroelastic coupling in which the fluid and flexible foil simultaneously affect each other's behavior. The project investigated relationships for the propulsors' thrust and efficiency performance to gain a better understanding of the dynamic interaction with the surrounding fluid. The analysis was conducted through reduction of the measured force and torque data. The experiments took place in a large recirculating water channel, using full span flexible propulsor models and a higher Reynolds number than previous flexible propulsor experiments. The propulsor pitched about a fixed axis at its quarter chord, with a six-axis load cell measuring the forces and torques on the shaft. The efficiency of the propulsor and the Coefficients of Thrust and Lift are presented as functions of both Strouhal Number and Stiffness Coefficient. The ensemble data will facilitate the engineering of fish-like propulsion systems for future application of this technology.

Published by Elsevier Ltd.

1. Introduction

While most marine vessels use traditional propellers and rudders for propulsion and handling, research points to the possibility of developing new capabilities by taking advantage of the unsteady dynamics associated with the organic movement of a fish (Lai et al., 1993; Lighthill, 1975; Read, 2001; Triantafyllou et al., 2004). Straying away from traditional propulsion and mimicking the motion of a fish may have a significant impact on the current doctrine of underwater propulsion techniques. Propellers have demonstrated their effectiveness at attaining high speeds through the water, but the associated rudders are only useful when there is a significant wash over the surface. At low speeds, ships can become more difficult to maneuver with this system. A fish, however, using coordinated, organic movement, can effectively turn and accelerate from a standstill to pursue prey or escape from a predator. Natural selection suggests that this means of propulsion is effective in hostile underwater environments. The complicated dynamics of the unsteady, coupled fluid-structural system make simulation or experimental replication of the interaction between the fish and the environment difficult. However, a simplified system that eliminates the biological feedback and reduces the motion down to a few key dynamic mechanisms may be able to produce the same performance as a fish in a way that is easier to mechanize.

* Corresponding author.
E-mail address: brownell@usna.edu (C.J. Brownell).

http://dx.doi.org/10.1016/j.jfluidstructs.2016.09.003
0889-9746/Published by Elsevier Ltd.

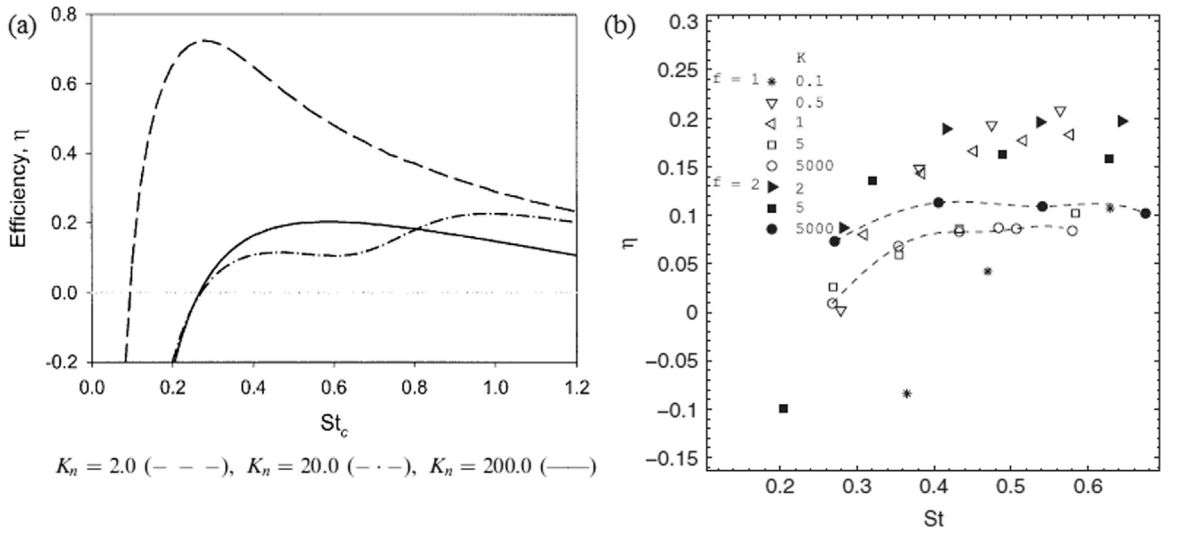

Fig. 1. Propulsor efficiencies for various Stiffness Constants and Strouhal Numbers for (a) the rigid heaving propulsor (Murray, 1999) and (b) the flexible flat plate propulsor (Dia et al., 2012). Figures are reproduced with permission from the authors.

Previous analysis of a basic rigid foil pitching about a fixed point found that by varying the frequency and amplitude of the rigid pitching propulsor, the number and type of vortices shed per oscillation into the wake can vary significantly (Koochesfahani, 1987; Schnipper et al., 2009). This analysis also shows that the vorticity of the wake directly relates to the amount of thrust and lift produced while the foil oscillates. Other research incorporated a heaving motion in which the foil pitches about a point moving perpendicular to the free-stream flow (Anderson et al., 1998; Scherer, 1968; Schouveiler et al., 2005). To produce optimal thrust, the phase between the pitching and heaving motions must synchronize. This coordination further complicates the propulsor actuation, but the mechanization can be simplified by connecting the pitch point to a spring to allow passive heaving (Murray and Howle, 2003). This configuration takes advantage of the natural tendency to heave and allows the variable spring stiffness to contribute to the thrust production and efficiency of the system.

Research on flexible propulsors, including pitching plates (Dia et al., 2012; Dewey et al., 2013; Murray, 1999) and flapping foils (Bose, 1995; Prempraneerach et al., 2003; Dia et al., 2012) has shown that flexibility yields increases in efficiency under certain conditions. Dia et al. investigated a fixed pitch point with a naturally delayed phase heave downstream on a flexible propulsor (Dia et al., 2012). Efficiency results from models of both heaving rigid (Murray, 1999) and flexible (Dia et al., 2012) propulsors are shown in Fig. 1. These graphs indicate that there are points of optimization within the data set that will result in the most efficient performance if the propulsor or spring has the correct pairing of oscillation frequency and stiffness. By creating a ratio of elastic force to hydrodynamic lift force, Prempraneerach et al. (2003) defined a flexibility parameter for scaling the effects of flexibility on a propulsor. In the review by Triantafyllou et al. (2005), the flexibility parameter is defined as $\Delta = (45/2)(\rho C_L U^2/E)(c/h)^3$ where ρ is the fluid density, C_L is the lift coefficient, U is the free-stream velocity, E is the Young's modulus, c is the chord, and h is the mean foil thickness; an optimal value of $\Delta = 1/3$ is provided. Dewey et al. (2013) present experimental results on pitching flexible panels with a stationary leading edge fairing. They develop new scaling laws for thrust and efficiency for flexible panels, and show experimental verification of these laws. Furthermore, Dewey et al. (2013) assert that achieving efficient propulsion with flexible propulsors requires both operation within the optimal Strouhal range and operating near the structural resonant frequency of the foil.

Few studies have explicitly examined the role of Reynolds number on the performance of foil propulsors. The highest Reynolds numbers from prior experiments are approximately 4×10^4 (Anderson et al., 1998; Schouveiler et al., 2005), while Reynolds numbers for marine organisms may be $Re > 10^8$ (Vogel, 1994). Likewise, the Reynolds number for an underwater vehicle may be significantly higher than existing laboratory experiments. Within the range of sub-critical Reynolds numbers, the impact of Reynolds number is understood to be through influence of the (friction) drag coefficient on the foil (Triantafyllou et al., 2005). While drag and thrust forces cannot be easily separated in an experiment, higher Reynolds numbers should produce lower drag coefficients and therefore higher efficiency, all else being equal. Comparisons of experimental thrust data to inviscid theory show an offset, relatively constant across a range of Strouhal numbers, that can be attributed to the difference in drag coefficient (Anderson et al., 1998).

The work presented here tests the two dimensional case of a pitching flexible propulsor, pitching about a fixed point at its quarter chord. The Reynolds numbers for these experiments extend to $Re = 3 \times 10^5$, still below the critical Reynolds number but almost an order of magnitude higher than what is found in other experiments. Foil flexibilities span the optimal range of the flexibility parameter, and the thrust and efficiency were measured with respect to the non-dimensionalized foil stiffness, water velocity, and oscillation frequency.

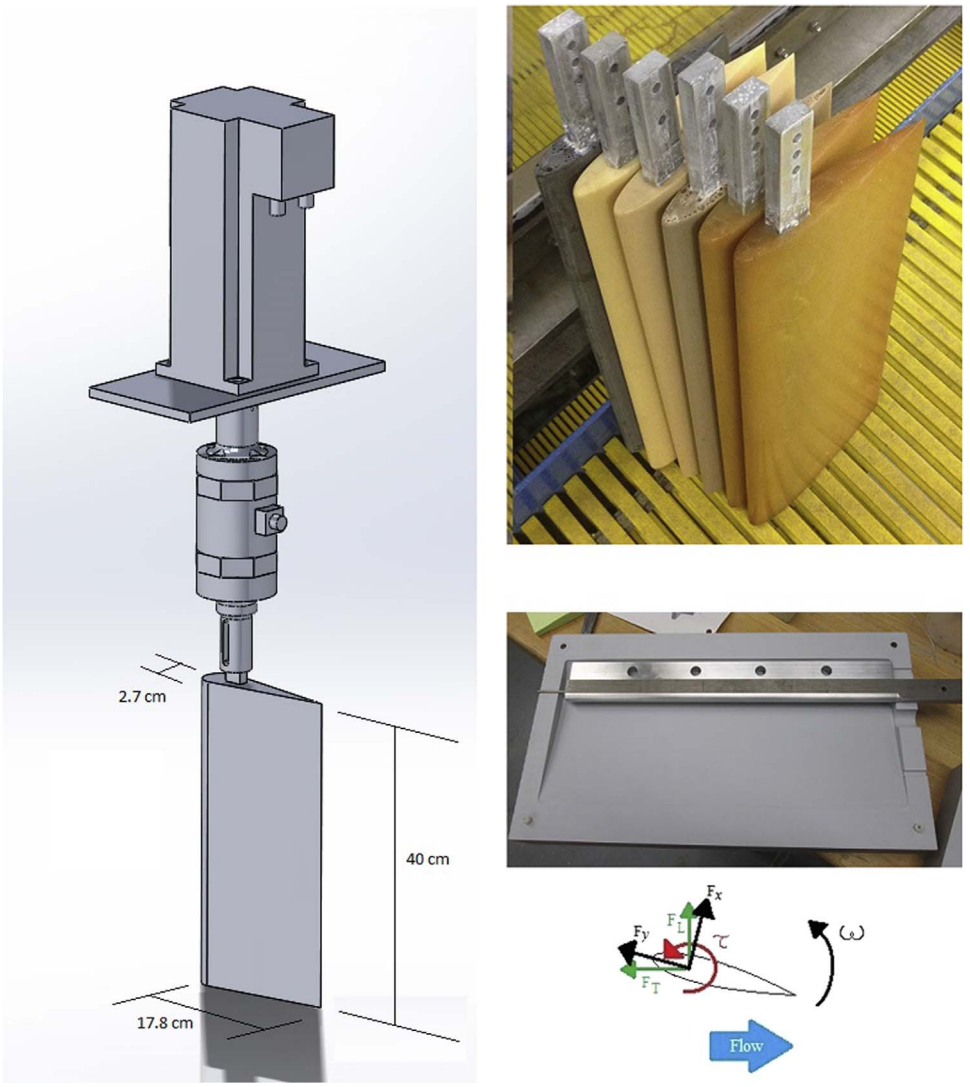

Fig. 2. Clockwise from left: Schematic of the testing apparatus outfitted for the water channel; the six foils with protruding aluminum backbone; the aluminum backbone in the foil cast, and the coordinate system for the experiments.

2. Experimental details

The dimensionless parameters used for this analysis include the Reynolds Number, $Re = \rho Vc/\mu$, Strouhal Number, $St = fL/V$, Stiffness Constant, $K = EI/0.5\rho V^2 c^3$, and Swept Distance, $S = L/c$, where ρ is the fluid density, V is the free-stream velocity, c is the chord length, μ is the fluid dynamic viscosity, f is the oscillation frequency, L is the swept length of the trailing edge of the foil, E is the modulus of elasticity, and I is the 2D moment of inertia.

Fig. 2 shows a scaled schematic of the setup for the testing of the pitching flexible propulsor. The experiment was conducted in a large water channel with a 40 cm $\times$ 40 cm cross section along a length of 150 cm. Within the test section, water flows over a full span foil, which is oscillating according to specified frequencies programmed into the motor. The load cell on the shaft between the motor and foil measures the forces and torques acting on the propulsor. A grounding board, present between the foil and foil bracket and covering the entire test section, prevents free-surface interaction with the pitching foil and reduces span tip vortex formation to test the 2D flow case. The tip gaps between the foil and the upper and lower surfaces were 3 mm or less. The apparatus rigidly mounts the motor on the sides of the water channel, connects through the load cell, and holds the foil in the proper position within the test section.

The foils were a standard NACA0015 airfoil with a span of 40 cm and a chord length of 17.8 cm. The maximum thickness of the foil is 2.7 cm, making the chord to thickness ratio $c/h = 6.6$. Because of the relatively thick, rigid foils, the mass properties of the foil are assumed to be insignificant. To confirm this, the structural resonant frequencies of the foils were estimated using COMSOL Multiphysics, and found to range from 7 Hz to 37 Hz. These frequencies are higher than the

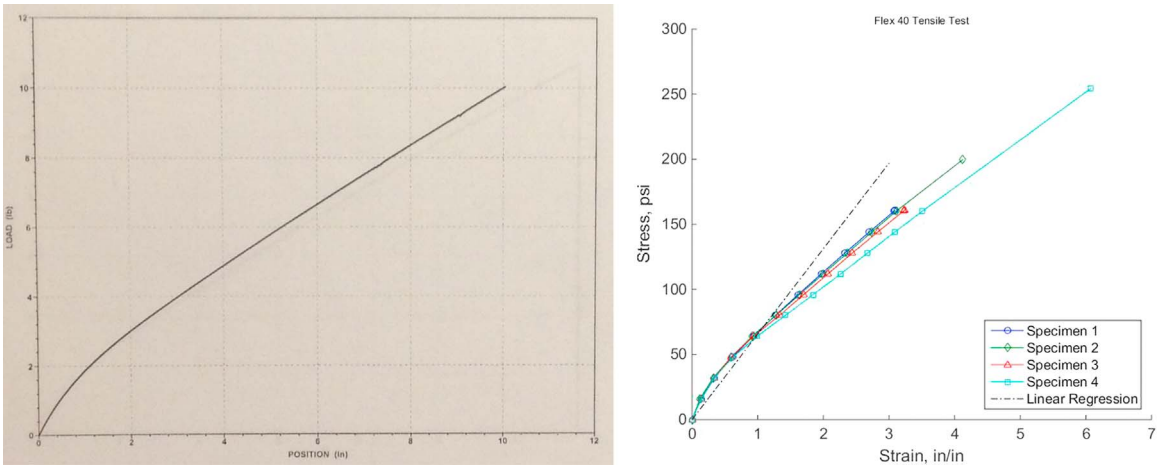

Fig. 3. Load–displacement plot from the tensile test for the Flex 40 Alumilite material and the linear regression to calculate the modulus of elasticity.

highest frequencies seen in the present experiments. The foils were made of six different grades of Alumilite Flex urethane poured into a cast (see Fig. 2) around an aluminum backbone which maintained rigidity in the front quarter chord of the foil. The modulus of elasticity of the foils depends on the grade of urethane used. The modulus was determined through tensile testing of "dog bone" specimens made from the same material as each of the foils. The dog bone and tensile testing procedure come from ASTM D638 for tensile testing of plastics and D412 for testing of rubber elastomers, respectively (ASTM Standard D412, 2013; ASTM Standard D638, 2010). The tensile tests generated load–displacement curves which were converted into stress–strain diagrams. A linear regression of the stress–strain curve determined the slope which graphically represents the modulus of elasticity (Fig. 3). Although the tensile test results show a nonlinear relationship, the maximum strain experienced by any foil was estimated to be 9% and the linear regression was applied over this range for all material samples. While the resulting moduli do not provide a complete description of the stress-strain relationship for a given foil, they provide an accurate benchmark for the stiffness comparisons between the foils used in this experiment.

Table 1 provides the results of the material testing with the modulus of elasticity for each material. The Moduli span several orders of magnitude for the flexible materials and the rigid material is 2.3 orders of magnitude stiffer than the stiffest, Flex 80 foil. The manufacturer's comparison is provided by the Alumilite Corporation to give an idea of the approximate stiffness of the Flex materials.

The six-axis load cell (AMTI SP4D-3 K-13970) measures forces and torques in the x, y, and z directions. The forces of interest during the experiment were the x (wall normal) and y (chordwise) forces which were transformed into the lift and thrust forces depending on the instantaneous angular position of the foil. These forces determined the power out and efficiency of the propulsor. In the z-axis, the load cell measured the torque on the propulsor shaft, which was integrated with the rotational velocity to determine the input power and efficiency. While only these three outputs were paramount to the analysis, all six axes of the load cell were recorded for each run to compensate for crosstalk between the axes within the load cell. A sampling rate of 300 Hz resolved the forces and torques measured throughout the entire cycle of oscillation, which was never more than 4 Hz.

The motor (Baldor AC brushless servo, BSM100N-4250AA) manipulated the angular position of the propulsor using a proportional/integral/derivative (PID) controller with a sine wave programmed as the commanded input. The device used a 480 V powered iterative feedback loop so that the motor oscillated the foil with minimal lag by adjusting the torque on the shaft as necessary to counteract the forces in the surrounding fluid. The bandwidth of the PID controller was estimated to be 8 Hz. The amplitude of the oscillation angle was the same for all experiments, $\pm 15^{\circ}$, and flow imaging experiments confirmed that the full amplitude was achieved for all run conditions. The angular amplitude selected is in line with previous research on oscillating propulsors (Anderson et al., 1998; Dewey et al., 2013; Prempraneerach et al., 2003) and near an

Table 1
Material properties.

Foil material	Modulus of elasticity (Pa)	Manufacturer comparison (Alumilite Corporation)
Rigid	3.00E+09	N/A
Flex 80	1.45E+07	Roller blade wheel
Flex 70	7.20E+06	Car tire
Flex 60	2.13E+06	Shoe sole
Flex 40	5.31E+05	Wine cork
Flex 30	4.00E+05	Soft rubber gasket

Table 2
Parameter space.

		Minimum value	Maximum value
Independent variables	Flow velocity, m/s	0.1	1.5
	Oscillation frequency, Hz	2.0	3.6
	Modulus of elasticity, Pa	4.0E+5	3.0E+9
Dimensionless parameters	Reynolds number, Re	3.0E+4	3.0E+5
	Strouhal Number, St	0.1	1.5
	Stiffness Coefficient, K	1.0E−1	6.0E4
	Swept length, S	1.5	1.5

optimal value for propulsive efficiency (Schouveiler et al., 2005). Because the flow had a finite cross-section, the angular amplitude was also limited to prevent significant blockage of the fluid flow in the channel.

The parameter ranges for stiffness and Strouhal Number used for the analysis, provided in Table 2, were determined based on evaluations of the current literature (Dewey et al., 2013; Prempraneerach et al., 2003; Rohr and Fish, 2004) as well as some limitations of the testing apparatus. Within these ranges, it was expected that local peaks in thrust and efficiency would be found at intermediate values of the Strouhal Number and Stiffness Constant ranges shown in Table 2. As an example, the Flex 60 foil operating in a free-stream velocity of $U=0.33$ m/s gives a value of the previously defined flexibility parameter near the optimal value of $\Delta = 1/3$.

The fluid velocity was set using eight different flow speeds logarithmically spaced from 0.18 m/s to 1.4 m/s. Seven oscillation frequencies were also logarithmically spaced between 2.0 Hz and 3.6 Hz. Each flow speed was paired with each oscillation frequency for a total of 56 Strouhal Numbers spaced from 0.1 to 1.3. The 56 Strouhal Numbers were tested for each of the six flexible foils, for a grand total of 336 unique run conditions.

Each experimental run was performed for a duration of 30 s, with a data acquisition rate of 300 Hz. In the data reduction process, the initial 2 s of data was truncated to remove any possible transients. The end of the data was also truncated to ensure an integer number of oscillation periods per run. At the extremes, runs with a 2 Hz oscillation rate were truncated at $t=29.500$ s for a total of 55 periods and 150 points per period, and runs at 3.6 Hz were truncated at $t=29.778$ s for a total of 100 periods and 83.3 points per period.

Dye injection was used to perform a brief qualitative flow visualization of the experimental setup. The dye visualization, shown in Fig. 4, demonstrated that the setup was correctly configured to generate vortices in the wake behind the propulsor. The images shown are from the Flex40 foil with St=0.6. Analysis of the wake vortex patters and the associated deposition of momentum into the fluid gave qualitative information on the transition from negative to positive thrust production. These observations were confirmed with the data from the load cell.

3. Results and analysis

Because the load cell rotated with the foil, it measured forces parallel and perpendicular to the chord of the foil. These forces were transformed to a coordinate system relative to the flow using the instantaneous angle of attack of the foil. These forces are non-dimensionalized into the Coefficient of Thrust, C_T, and Coefficient of Lift, C_L,

$$C_T = \frac{F_T}{\frac{1}{2}\rho V^2 cb}$$

and

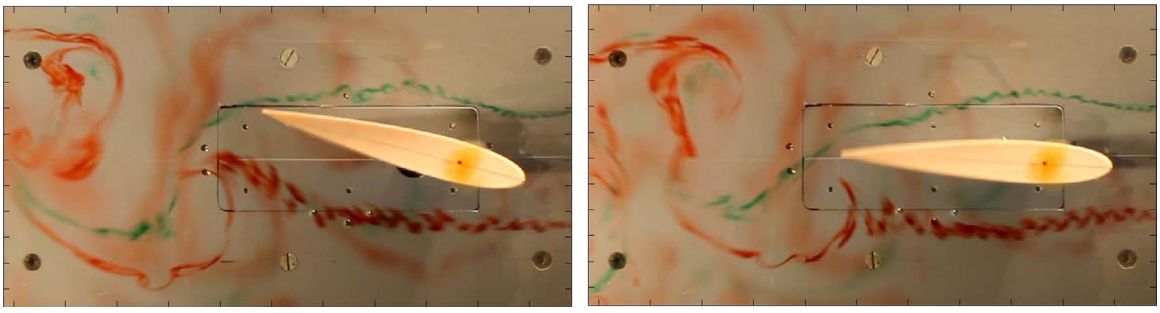

Fig. 4. Dye injection to confirm the vortex shedding regime. Images are of the Flex 40 foil at St=0.6.

$$C_L = \frac{F_L}{\frac{1}{2}\rho V^2 cb}$$

where b is the foil span. A negative thrust force means that the drag on the propulsor is larger than the thrust it produces. Because of the equal and opposite relationship of thrust and drag in this experiment, the thrust was conventionalized as a positive force to simplify the analysis of collected data and reflect the goals of the experiment.

The torque from the load cell was integrated over a full period of oscillation with the instantaneous angular velocity to determine the power being delivered to the system by the motor, P_{in}. The thrust was also integrated over a full period of oscillation with the free-stream velocity to determine the power out, P_{out}. The power in and power out are used to determine the efficiency, η, specified by:

$$P_{in} = \frac{1}{T}\int \tau\omega dt,$$

$$P_{out} = \frac{1}{T}\int F_T V dt,$$

and

$$\eta = \frac{P_{out}}{P_{in}}$$

where T is the period of foil oscillation, τ is the shaft torque, ω is the angular velocity, and t is time.

Preliminary tests showed that some data smoothing would be required. In the ideal case with one shed vortex per cycle, the measured force perpendicular to the foil would be symmetric, and would consist of one dominant peak and trough per cycle, corresponding to the equal and opposite forces on the foil as it pushes through the water. Between the peaks and troughs, the force should gradually drop through zero near the maximum extent of the oscillations as the foil stops and proceeds in the opposite direction. This would produce an ovular shape as the force traces counterclockwise through its maximum, minimum, and respective zeros. The unfiltered data, however, shows several additional oscillations that indicate several other local peaks during the oscillation. The cause of these additional peaks was identified as the motor shaft cogging rather than moving smoothly through the oscillations. This cogging is caused by the preferred alignment of the permanent magnets in the motor to the metal in the stator windings. This behavior is common among high power, DC brushless motors, especially when performing motions that require only a small percentage of their maximum capabilities. In motion profiles that require more effort, the power into the motor can more easily overcome the preferred alignment and move smoothly between specified angles. Fig. 5 shows the lift force on the foil measured with respect to its angular position without (left) and with (right) a filter.

A software-based zero phase low-pass filter with a cutoff frequency five times the dominant oscillation frequency was applied to the data. This cutoff frequency allowed for the inclusion of phenomena that occur up to four times per cycle during the oscillation. This filter was chosen because of the high frequency, periodic nature of the cogging. While the cogging phenomena and the filtering to remove it affects instantaneous force measurements, it has little impact on the values of averaged quantities. The overall uncertainty in load cell measurements is the primary source of error for averaged quantities, as will be discussed later.

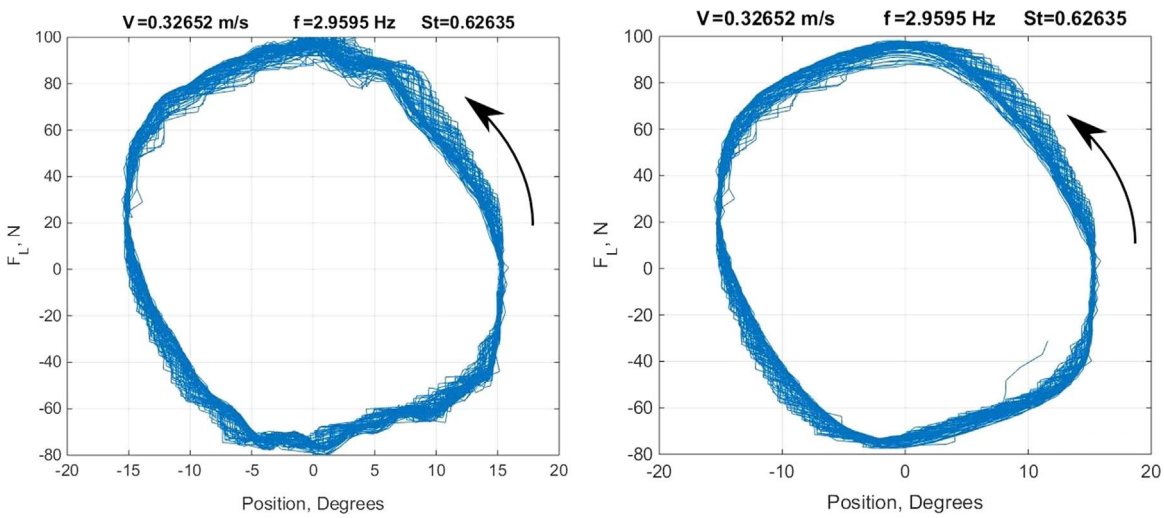

Fig. 5. Unfiltered (left) and filtered (right) force data. Arrows show direction of forward time.

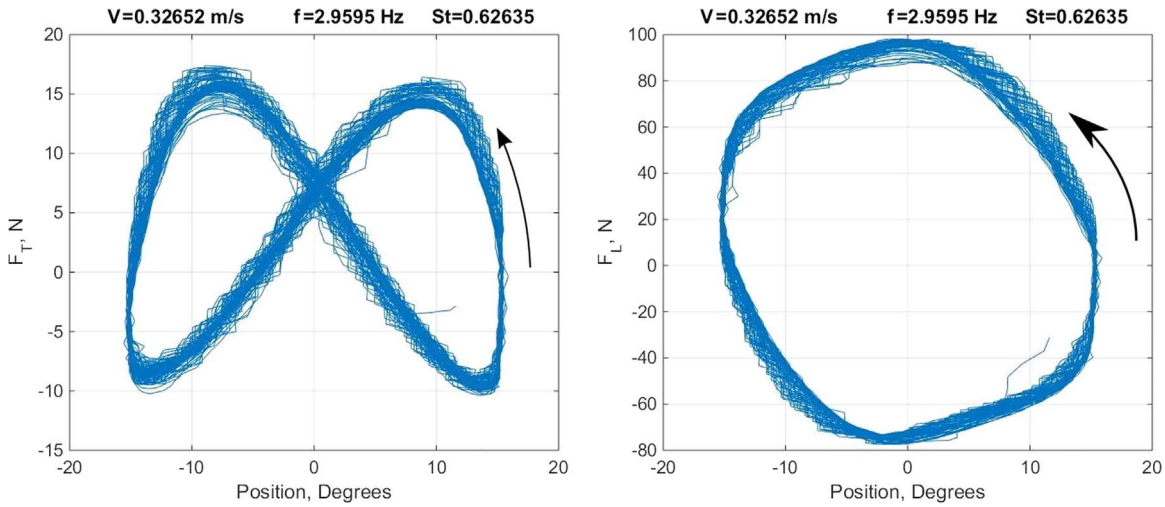

Fig. 6. Phase plots of thrust (left) and lift (right) forces. Arrows show direction of forward time.

The forces in line and perpendicular to the foil chord were transformed into the streamwise thrust and perpendicular lift forces based on the instantaneous position of the foil. Fig. 6 displays the transformed data represented as the forces of thrust and lift. The arrows in the figure show the direction of forward progression in time. The shape of the thrust plot reveals several important pieces of information about the oscillation performance. The peaks of the thrust plot lie at about 15 N while the lowest points only go down to about -10 N. The negative value of the thrust indicates that the fluid is pushing the foil backwards along with the flow rather than forward against the flow. This is the result of drag on the foil as well as the force required by the foil to push into the flow to reach the maximum 15° angle on either side of its oscillation. However, because the foil is being considered as a propulsor attached to a vehicle rather than a vehicle itself, all negative forces are generically referred to as a drag that is innate to its oscillation through a flow. Regardless of naming convention, this asymmetry indicates that the foil generates higher thrust as it begins its swing than it creates drag at the end of its swing in each direction.

Because the power developed by the system involves an integral of the thrust multiplied by the free-stream velocity, the amount of area above and below the zero force axis on the thrust plot is related to whether the oscillation had a positive or negative output power into the system. This is not a perfect correlation because the graphs do not indicate the angular velocity of the foil being highest near the 0° point and zero at the 15° point. Since the integral is taken with respect to time, the amount of time spent at any given force in the plot is significant. The forces at angles further from 0° will have a higher weight in the integral due to the lower angular velocity at those points. However, the graph still provides an initial look at the power performance of the propulsor as the sign of the power in turn determines the sign of the efficiency of the oscillation. In the case shown in Fig. 6, the area above the zero force axis is visibly larger than the area below the axis. In this case, the efficiency is calculated to be 8.34%. The remaining power is lost due to unproductive water movement and mechanical losses.

In general, a higher proportion of area above the axis than below it corresponds to a positive value for efficiency. Fig. 7 displays the thrust and lift plots for a lower Strouhal Number ($St = 0.4$, $f = 2$ Hz) oscillation of the relatively flexible Flex 30 foil. Visibly, the thrust plot is nearly symmetrical about the zero-force axis, which corresponds to its -0.1% efficiency. Zero efficiency means that the foil is taking just as much power out of the fluid through drag as it is generating through its thrust production. Further increases in the area below the axis, particularly in regions away from the 0° point where the angular velocity of the foil is low, correlate with negative efficiencies that result in a net loss of power from the fluid.

The amount of thrust produced by the foil for a given parameter set can be characterized by the Coefficient of Thrust, C_T. Fig. 8 shows the Coefficients of Thrust calculated for each foil and for each Strouhal Number. The Thrust Coefficients for each foil follows an approximately exponential growth as the Strouhal Number increases. At the lowest Strouhal Numbers, some of the Thrust Coefficients are negative, which indicates that the foil is producing more drag than thrust in the oscillation. The negative Thrust Coefficient also corresponds to a negative efficiency. The trends seen in the data indicate that the most rigid foils produce greater thrust than the more flexible foils for any given Strouhal Number.

While the thrust graphs can be compared visibly to determine relative performance, it is not possible to quantitatively determine the efficiency of the oscillation based on the thrust alone. The efficiency also takes into consideration the amount of power being put into the foil through an integration of the torque on the shaft multiplied by its instantaneous angular velocity. The torque on the shaft is due to the forces perpendicular to the foil chord that act at a center of pressure behind the shaft axis, which result in a moment applied to the shaft.

Fig. 9 shows the plots of the torque multiplied by the angular velocity plotted against the angular position. The left plot is from the same 8.34% efficiency data set as seen in Fig. 6, and the right plot is from the zero efficiency run in Fig. 7. Analysis of

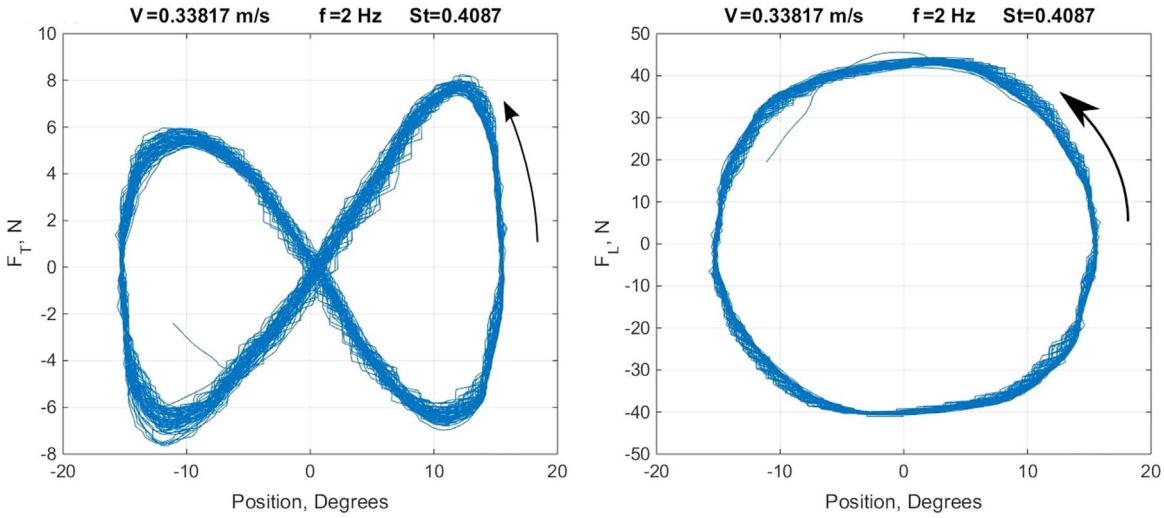

Fig. 7. Thrust and lift forces from a lower Strouhal Number run with Flex 30 foil.

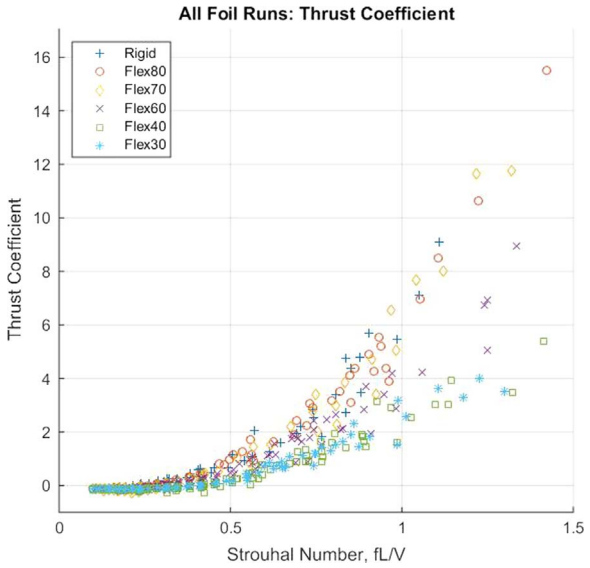

Fig. 8. Thrust coefficients for all foils.

these plots gives similar insights into the power being input into the foil through the shaft. For the high efficiency oscillation, the data trace through roughly the same path whether the foil is moving from its center position to its maximum angular position or vice versa. This pattern is primarily seen in runs with higher Strouhal Numbers where the velocity of the fluid is small compared to the frequency of the foil. The water is not moving fast enough to induce any significant additional drag relative to the dynamic forces being generated in the oscillation.

The right plot displays the shaft torque multiplied by its angular velocity from zero efficiency case of the Flex 30 foil shown in Fig. 7. While the flow speed is approximately the same between the two cases, this oscillation has a lower frequency, which results in a lower Strouhal Number. In this case, the combined decreased angular velocity and resulting torque necessary to rotate the shaft result in values about one third of the previous case. The two arches also separate as a result of the maximum torque occurring earlier in the foil's swing from maximum angle to the zero angle. The lower relative torque is likely due to the foil not moving fast enough to sustain a positive pressure in advance of its angular swing. Changes in vortex formation and shedding at these lower Strouhal Numbers is likely important also, but this cannot be confirmed without further flow visualization. With the integrated torque multiplied by the angular velocity in the denominator of the efficiency equation, the larger values in these plots result in lower efficiencies for the same thrust outputs. The total efficiency can be increased by either increasing the power being output by the foil or decreasing the power input into the foil without changing the opposing power input or output power, respectively.

Fig. 10 shows the calculated rigid foil efficiency vs Strouhal number, presented with errorbars. The error was estimated using the uncertainty of the load cell measurements, assumed to be the primary source of error for time-averaged

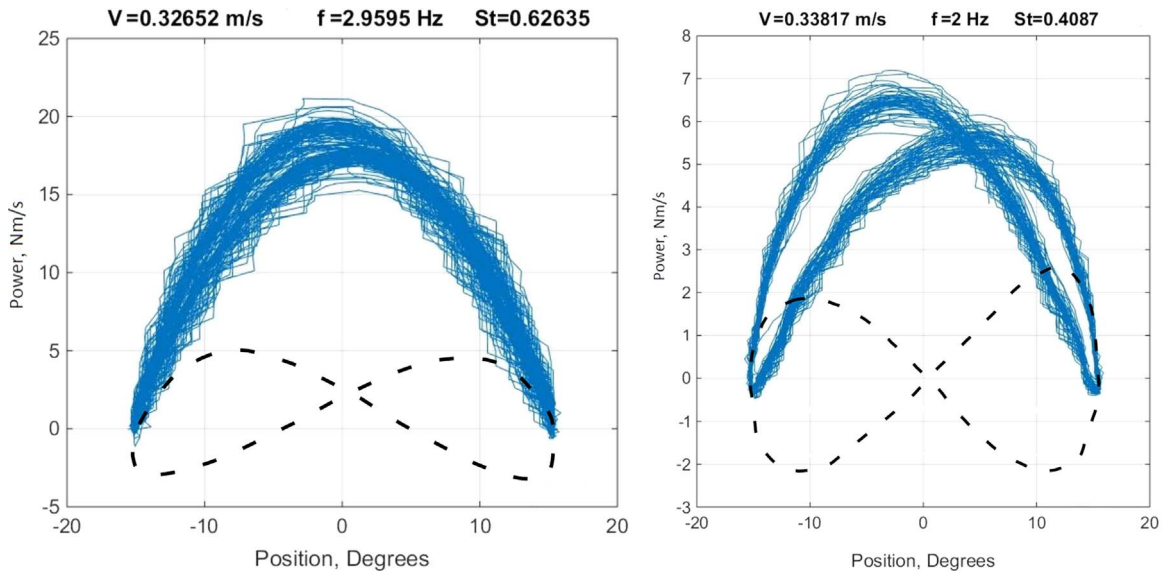

Fig. 9. Calculated shaft power for high (left) and low (right) Strouhal Number oscillations. The dashed lines represent a trace of the measured power out from the foil for each case.

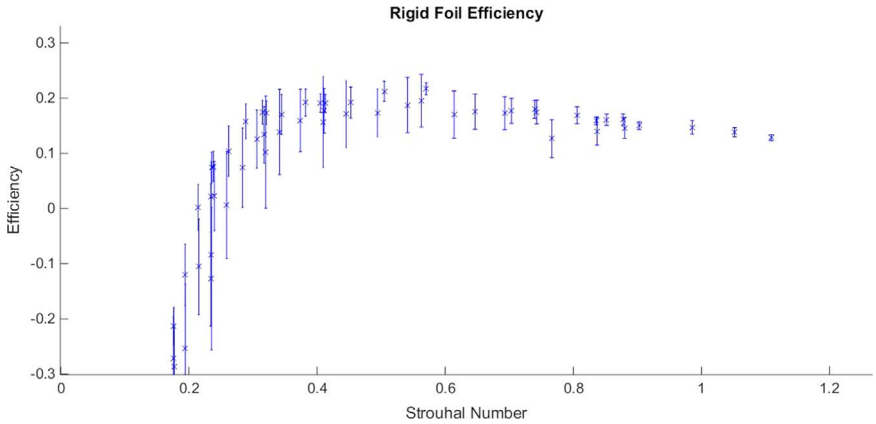

Fig. 10. Efficiency for the rigid foil with error bars.

quantities. The load cell uncertainty of 0.2% of full scale becomes relatively large for conditions where the overall magnitude of measured forces is small. This results in larger uncertainty for efficiencies near zero and for lower Strouhal Numbers in general.

Fig. 11 compares the predicted results from the coupled inviscid numerical model developed by Murray for the uniform thickness and tapered rigid propulsors (Murray, 1999; Murray and Howle, 2003). The numbers in the legend correspond to each of the eight flow velocities tested. The general trends shown by both data sets are very similar. Both increase steeply from negative efficiencies, level out at a maximum efficiency, and slowly decrease linearly with increasing Strouhal Number. The model under-predicts the efficiency at low Strouhal Numbers, and over-predicts at high Strouhal Numbers. The maximum efficiency is also lower for the experimental data, but this maximum occurs at a lower Strouhal Number than predicted by the numerical model. Some of the differences between model and experiment may be due to the formation of leading edge vortices, which were found by Anderson et al. (1998) to result in efficiencies that, under certain conditions, exceed those predicted by inviscid theory. While the numerical model does not perfectly predict the rigid foil performance, the experimental data show that the model can be used as an initial approximation for application of rigid propulsors.

Fig. 12 shows the efficiencies plotted for all foils. In general, the foils with the higher Stiffness Constants had higher efficiencies for any given oscillation observed. The rigid foil had the highest efficiencies out of all the foils. The Flex 80, Flex 70, and Flex 60 foils all appeared to have results clustered just below the rigid foil on the efficiency plots. The Flex 40 and Flex 30 foils also clustered together, but there was a gap between their efficiencies and the efficiencies of the other cluster of foils.

Table 3 provides the approximate values of the maximum measured efficiency and its corresponding Strouhal Number, the Strouhal Number where the spline function crosses the zero efficiency line, and the slope of the efficiency data after the peak is reached. Depending on the foil, the maximum efficiency is reached at a Strouhal Number between 0.4 and 0.6. In

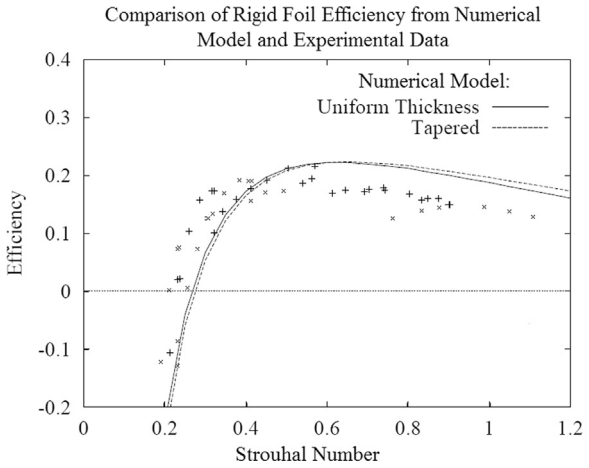

Fig. 11. Efficiency for the rigid foil oscillations compared to predictions from numerical model (Murray, 1999).

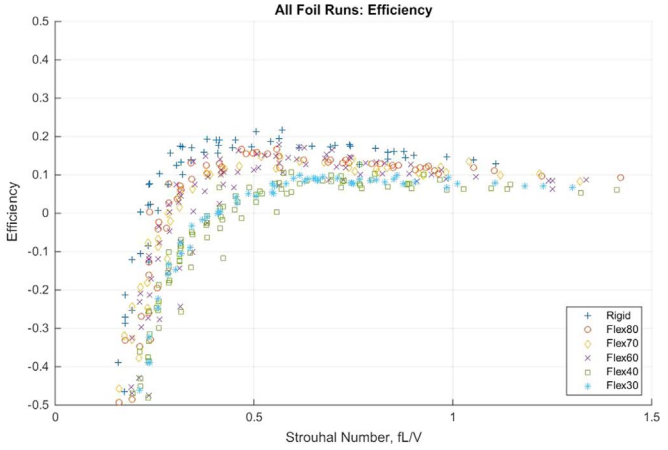

Fig. 12. Propulsive efficiency for all foils and Strouhal Numbers.

Table 3
Peak efficiencies.

Foil	Max efficiency, η (%)	St at max η	Strouhal at $\eta = 0$	Slope
Rigid	21.69	0.57	0.23	−0.16
Flex 80	16.77	0.56	0.28	−0.09
Flex 70	14.70	0.52	0.30	−0.08
Flex 60	17.81	0.56	0.33	−0.12
Flex 40	12.74	0.76	0.42	−0.10
Flex 30	9.94	0.62	0.42	−0.05

general, the more rigid foils reach their maximum efficiency at lower Strouhal Numbers than the more flexible foils. As a result, the foils with the higher Stiffness Constants peak in efficiency at lower oscillation frequencies. With lower oscillation frequencies at the peak, there is less power required to be input into the foil, which in turn gives a higher efficiency. After the peak in efficiency, all of the foils show consistent decreasing trends in efficiency. The decrease for the more rigid foils, which have higher peaks, is steeper than the more flexible foils. As the Strouhal Number increases from values below 0.2, the efficiency rises from extremely negative efficiencies. These low Strouhal Number oscillations show the biggest difference in efficiency performance between foils. For example, the same Strouhal Number that gives a efficiency of zero for the rigid foil gives a −50% efficiency for the Flex 30 and Flex 40 foils. Increases in Strouhal Number from 0.3 to 0.5 cause marginally smaller increases in efficiency as the trend lines become less steep.

Fig. 13 displays the same efficiency information, but with the Stiffness Constant plotted logarithmically on the third axis. The data make a surface that has a near linear gradient causing a proportional increase in efficiency at any given Strouhal Number with a logarithmic increase in Stiffness Constant.

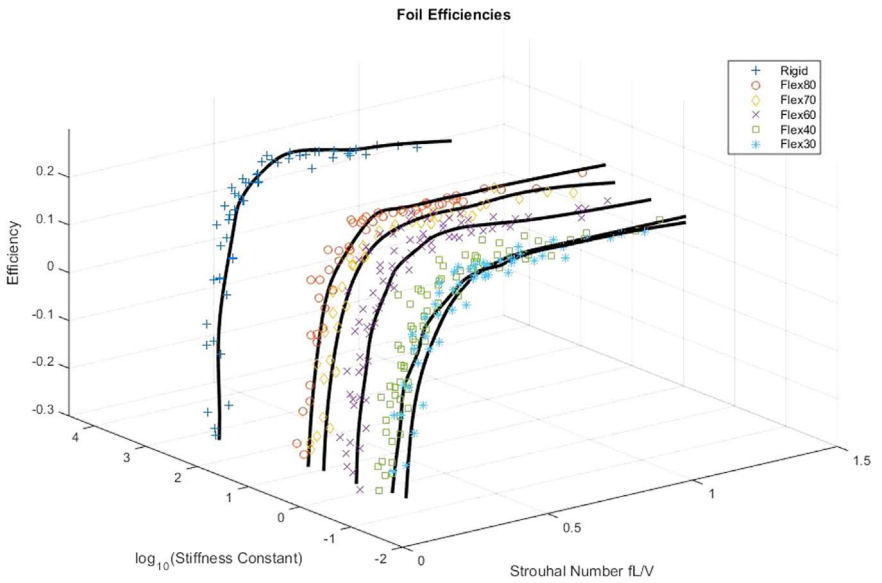

Fig. 13. Three-dimensional plot of Strouhal Number, Stiffness Constant, and propulsive efficiency, with best fit lines for each foil.

4. Conclusions

Although the majority of previous research indicated that a flexible foil should see increased performance over its rigid counterparts (Bose, 1995; Dewey et al., 2013; Prempraneerach et al., 2003), this result was not found for the geometry and parameter space used here. The high Reynolds numbers used in the current tests are unlikely to be the cause of this discrepancy. As Reynolds number varied within these experiments by an order of magnitude, little dependence was observed. The findings here are consistent with an understanding of the role of sub-critical Reynolds number being limited to its effect on drag coefficient. One possible explanation for the discrepancy in efficiency is the geometry and motion of the foil. Previous experiments that used only a pitching motion either included a fixed leading edge (Dewey et al., 2013) or used smaller pitching amplitudes (Koochesfahani, 1987). The relatively large effective angle of attack in the current experiment may have disrupted the interaction of leading edge vortices interacting with wake vorticity in a way that leads to efficient propulsion.

The general trends of thrust and efficiency measured as a function of Strouhal Number match those of numerical models, and are consistent with results from the literature. The good comparison between simulation and experiment for the rigid foil efficiency increases the confidence in the results, and experimental error is shown to be small, particularly for cases with larger measured thrust. The data herein provides a framework to estimate the performance of flexible propulsors for application to marine vehicles in the future. However, the discrepancy in the trends of efficiency between the various Stiffness Constants must be resolved before flexible propulsor technology can be productively applied.

Acknowledgments

The authors would like to thank the United States Naval Academy Hydrodynamics Laboratory, and the USNA Trident Scholar Program for their assistance.

This research did not receive any specific grant from funding agencies in the public, commercial, or not-for-profit sectors.

References

Alumilite Corporation. Online ⟨http://www.alumilite.com/store/pg/46-Casting-Resins.aspx⟩.

Anderson, J.M., Strietlien, K., Barrett, D.S., Triantafyllou, M.S., 1998. Oscillating foils of high propulsive efficiency. J. Fluid Mech. 360, 41–72.

ASTM Standard D412, 2013. Standard Test Methods for Vulcanized Rubber and Thermoplastic Elastomers Tension, ASTM International, West Conshohocken, PA.

ASTM Standard D638, 2010. Standard Test Method for Tensile Properties of Plastics, ASTM International, West Conshohocken, PA.

Bose, N., 1995. Performance of chordwise flexible oscillating propulsors using a time-domain panel method. Int. Shipbuild. Progr. 42, 281–294.

Dewey, P.A., Boschitsch, B.M., Moored, K.W., Stone, H.A., Smits, A.J., 2013. Scaling laws for the thrust production of flexible pitching panels. J. Fluid Mech. 732, 29–46.

Dia, H., Luo, H., Ferreira de Sousa, P.J.S.A., Doyle, J.F., 2012. Thrust performance of a flexible low-aspect-ratio pitching plate. Phys. Fluids 24, 101903.

Koochesfahani, M.M., 1987. Vortical patterns in the wake of an oscillating airfoil. In: AIAA 25th Aerospace Sciences Meeting, AIAA-87-0111, Reno, NV, January.

Lai, P.S.K., Bose, N., MGregor, R.C., 1993. Wave propulsion from a flexible-armed rigid-foil propulsor. Mar. Technol. Soc. J. 30, 28–36.
Lighthill, J., 1975. Mathematical Biofluiddynamics. SIAM, Philadelphia.
Murray, M.M., Howle, L.E., 2003. Spring stiffness influence on an oscillating propulsor. J. Fluids Struct. 17, 915–926.
Murray, M.M., 1999. Hydroelasticity Modeling of Flexible Propulsors (Ph.D. Dissertation), Duke University, Durham, NC.
Prempraneerach, P., Hover, F.S., Triantafyllou, M.S., 2003. The effect of chordwise flexibility on the thrust and efficiency of a flapping foil. In: Proceedings. Unmanned, Untethered Submersible Technology, Durham, NH, August.
Read, D.A., 2001. Oscillating Foils for Propulsion and Maneuvering of Ships and Underwater Vehicles (SM Thesis), MIT, Cambridge, MA.
Rohr, J.J., Fish, F.E., 2004. Strouhal Numbers and optimization of swimming by odontocete cetaceans. J. Exp. Biol. 207, 1633–1642.
Scherer, J.O., 1968. Experimental and Theoretical Investigation of Large Amplitude Oscillating Foil Propulsion Systems, Technical Report No. 662–1, Hydronautics Inc., Laurel, MD.
Schnipper, T., Andersen, A., Bohr, T., 2009. Vortex wakes of a flapping foil. J. Fluid Mech. 633, 423–441.
Schouveiler, L., Hover, F.S., Triantafyllou, M.S., 2005. Performance of flapping foil propulsion. J. Fluids Struct. 20, 949–959.
Triantafyllou, M.S., Techet, A.H., Hover, F.S., 2004. Review of experimental work in biomimetic foils. IEEE J. Ocean. Eng. 29, 585–594.
Triantafyllou, M.S., Hover, F.S., Techet, A.H., Yue, D.K.P., 2005. Review of hydrodynamic scaling laws in aquatic locomotion and fishlike swimming. Trans. ASME Appl. Mech. Rev. 58, 226–237.
Vogel, S., 1994. Life in Moving Fluids. Princeton University Press, Princeton, NJ.